Steel and Composite Structures, *Vol. 29, No. 6 (2018) 767-779*
DOI: https://doi.org/10.12989/scs.2018.29.6.767

Topology optimization of steel plate shear walls in the moment frames

Mohammad Hadi Bagherinejad [a] and Abbas Haghollahi [*]

Faculty of Civil Engineering, Shahid Rajaee Teacher Training University, Tehran, Iran

(*Received July 25, 2018, Revised October 12, 2018, Accepted December 28, 2018*)

Abstract. In this paper, topology optimization (TO) is applied to find a new configuration for the perforated steel plate shear wall (PSPSW) based on the maximization of reaction forces as the objective function. An infill steel plate is introduced based on an experimental model for TO. The TO is conducted using the sensitivity analysis, the method of moving asymptotes and SIMP method. TO is done using a nonlinear analysis (geometry and material) considering the buckling. The final area of the optimized plate is equal to 50% of the infill plate. Three plate thicknesses and three length-to-height ratios are defined and their effects are investigated in the TO. It indicates the plate thickness has no significant impact on the optimization results. The nonlinear behavior of optimized plates under cyclic loading is studied and the strength, energy and fracture tendency of them are investigated. Also, four steel plates including infill plate, a plate with a central circle and two types of the multi-circle plate are introduced with equal plate volume for comparing with the results of the optimized plate.

Keywords: topology optimization; steel plate shear wall; moment frame; sensitivity-based method; method of moving asymptotes; SIMP method; perforated plate

1. Introduction

Steel plate shear walls (SPSW) have been considered as a suitable lateral resistance system in the recent decades. Features of this system include large energy dissipation capability, stable hysteretic behavior, they are much lighter and thinner in comparison with RC shear walls, fast in the erection process, applicable for the seismic retrofit, and have an integrated system in comparison to the braced systems. SPSWs resist the lateral loads through the diagonal tensile field. Diagonal tensile field generates yield points in the plate and consequently dissipates the induced energy by the lateral loads. Simultaneously with the forming of diagonal tensile field, buckling occurs in the other diagonal direction. The buckling causes the stiffness reduction and pinching behavior. According to the U.S. building codes (AISC360 2010), SPSWs should be used with the moment frames in order to mitigate the negative effects of plate buckling.

So far, many experimental studies have been done on the effects of holes on the SPSW behavior and various forms (see Fig. 1) have been proposed for the PSPSWs (Vian *et al*. 2009, Valizadeh *et al*. 2012, Matteis *et al*. 2016, Nassernia and Showkati 2017, Shekastehband *et al*. 2017). Also, there are a number of numerical and parametrical studies which were conducted on the PSPSWs. Chan *et al*. (2011) studied the effects of holes' diameter and plate thickness on the strength and stiffness of PSPSWs under a monotonic loading. Bhowmick *et al*. (2014) predicted the shear strength of the PSPSWs considering the change in the number and diameter of the holes and the aspect ratio of the frame.

Formisano *et al*. (2016) investigated the effects of the number and diameter of the holes, the plate thickness and the metal material on the PSPSWs based on an experimental model. Mustafa *et al*. (2018) studied the behavior of the un-stiffened, stiffened and stiffened with different openings shape based on an experimental model. Considering the conducted studies, a mathematical process is required for finding the optimal form of PSPSWs. Topology optimization (TO) could be an effective tool for determining the optimal form of PSPSWs. TO determines the best form of material configuration within a given design space, set of loads, boundary conditions and constraints.

TO can be divided into two parts: the first is the TO of skeletal or truss structures that has a discontinuous nature. In this case, the volume of the consumed material is very low in relation to the total volume of the structure (problems with a low volumetric ratio). The second part is the TO of continuous structures, which has continuous nature and a high volumetric ratio. The first numerical solution for TO problems of continuous structures, in which finite element method was assisted, was published by Bendsøe and Kikuchi (1988). In their paper, the homogenization method was used to solve the TO of structures. This method led to a significant increase in the researches. With the spread of computer science, TO was applied to the practical models and structures such as cantilever and simple beams (Roodsarabi *et al*. 2016a, b, Khatibinia *et al*. 2018), concrete structures (Gharehbaghi *et al*. 2016, Zhiyi *et al*. 2018), building outrigger truss (Lee *et al*. 2015), braced frames (Stromberg *et al*. 2012, Kutuk and

*Corresponding author, Ph.D., Assistant Professor,
E-mail: haghollahi@sru.ac.ir
[a] Ph.D. Candidate, E-mail: mh.bagherinejad@sru.ac.ir

ISSN: 1229-9367 (Print), 1598-6233 (Online)

(a) Shekastehband *et al*. (2017) (b) Matteis *et al*. (2016) (c) Vian *et al*. (2009)

Fig. 1 Experimental studies of PSPSW

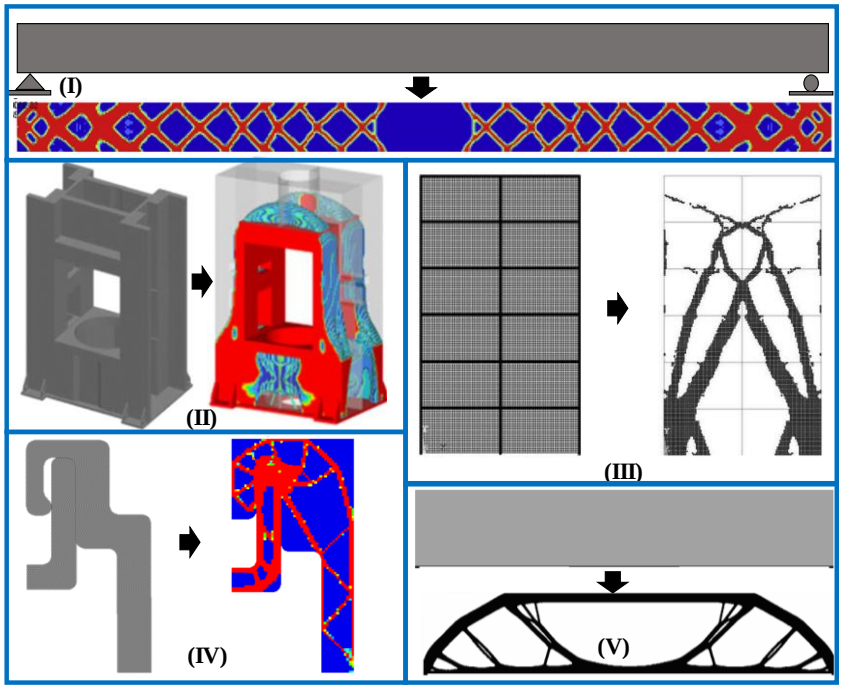

(I) Perforated steel beam (Tsavdaridis *et al*. 2015); (II) blanking press (Zhao *et al*. 2016); (III) Braced frame (Kutuk and Gov 2014); (IV) photovoltaic panel connector (Lu *et al*. 2017); (V) steel bridge (Jansseune and Corte 2017)

Fig. 2 Topology optimization studies

Gov 2014, Qiao *et al*. 2016, Zhou 2016), thin plate on elastic foundation (Banhd *et al*. 2018), single layer domes. (Gholizadeh and Barati 2014), railways (Das *et al*. 2011), space structures (Dehghani *et al*. 2016, Mashayekhi *et al*. 2016), bridges (Kutyłowski and Rasiak 2014, Jansseune and Corte 2017).

Also, robust programs were developed for TO such as TOSCA, Genesis, Altair Hypermesh, BESO and ParamMatters. Recently, a number of studies have been presented that optimize the topology of structures such as the roller bearing housing (Kabus and Pedersen 2012), buildings subjected to wind load (Tang *et al*. 2014), steel perforated I-sections (Tsavdaridis *et al*. 2015), a 12000kN fine blanking press (Zhao *et al*. 2016), photovoltaic panel connector (Lu *et al*. 2017), and steel railway bridge (Jansseune and Corte 2017) using these programs (see Fig. 2).

In this paper, TO is used to determine the optimum configuration of PSPSWs. The optimization is conducted by TOSCA (2013) that is combined with ABAQUS (2014). In the second section, a numerical finite element (FE) model is proposed based on an experimental model that was presented by Alavi and Nateghi (2013). In the third section, the TO methodology and parameters are described and defined. In the fourth section, the results of TO are presented and consequently, the optimum configurations of PSPSWs are obtained. In the fifth section, the cyclic behavior, energy dissipation and fracture tendency of the optimized models are investigated and compared with the other traditional models.

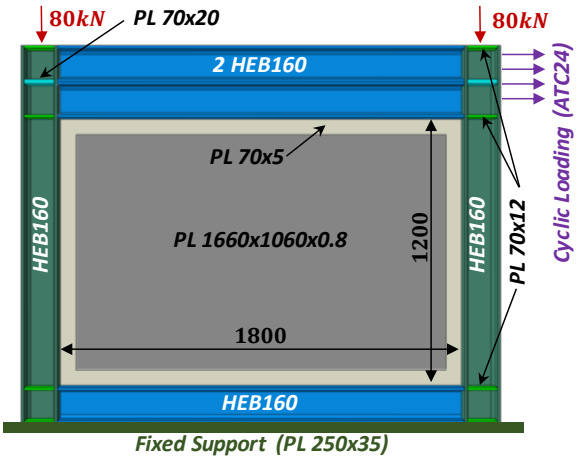

Fig. 3 Experimental model specifications (all dimensions are in millimeter)

Table 1 Material properties definition

Part	Elasticity Modulus (MPa)	Poisson ratio	Yield stress (MPa)	Ultimate stress (MPa)	Ultimate strain
PL1660×1060×0.8	2e5	0.3	250	400	0.2
Other parts	2e5	0.3	340	450	0.2

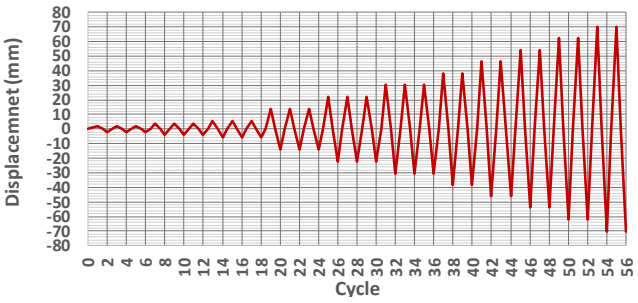

Fig. 4 ATC-24 loading pattern

2. Finite element modeling

The presented experimental model by Alavi and Nateghi (2013) is selected as the basic model for TO and analysis (see Fig. 3). As shown in Fig. 3, the model has a thin plate that is surrounded by a moment frame. The thickness of plate is equal to 0.8 mm. The material properties of the plate and frame are presented in Table 1. Nonlinear isotropic/kinematic hardening model is defined to simulate the behavior of materials. It is more accurate in predicting the behavior of steel under cyclic loading (ABAQUS 2014). The automatic stabilization is used for considering buckling, wrinkling and material instability. In the automatic stabilization method, a constant damping factor is utilized in any nonlinear quasi-static procedure based on the global equilibrium equation (Eq. (1)).

$$P - I - F_v = 0,\ F_v = cM^*v,\ v = \frac{\Delta u}{\Delta t} \tag{1}$$

where P and I is the external and internal forces respectively, F_v is viscous forces, c is a damping factor, M^* is an artificial mass matrix calculated with unity density, v is the vector of nodal velocities and Δu and Δt are the increment of displacement and time respectively.

The loading pattern is according to the ATC24 (1992) protocol presented in Fig. 4. Also, an axial load is imposed

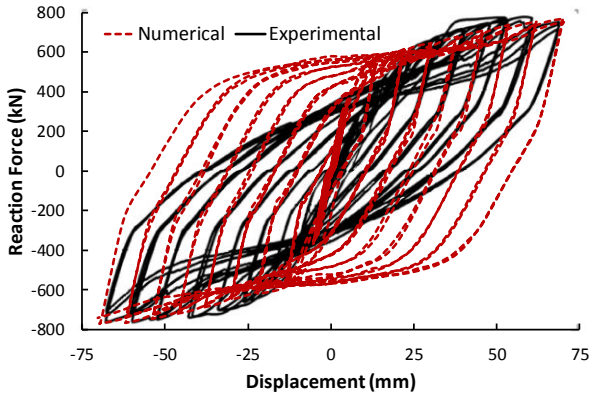

Fig. 5 Comparison of hysteresis behavior for numerical and experimental models

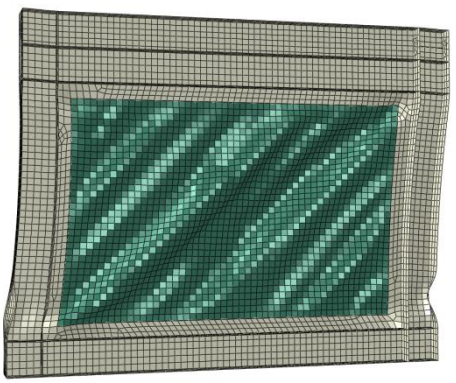

(a) Numerical model

(b) Experimental model

Fig. 6 Comparison of deformed shape

on both columns that is equal to 80 kN. The frame and plate are modeled with a 4-node shell element (S4R). The size of the mesh in the plate and frame is equal to 30 mm. The analysis is conducted in the static module and the effects of nonlinearity in material and geometry are considered. The cyclic curves of the numerical and experimental models are compared in Fig. 5. Also, the deformed shape of the plate is presented in Fig. 6 for both numerical and experimental models.

The results illustrate the proposed numerical FE model has appropriate compliance with the experimental model. The perfect conditions of finite element model especially in the beam-column moment connection, the using of tie connection replacing welded connection, and defined hardening material properties cause a reasonable difference (in the pinching behavior) between the cyclic curves of experimental and numerical models.

3. Topology optimization method

The objective function, constraint, conditions, stop criteria and the solution method are described in this section. Based on the proposed finite element model in the previous section, the effects of nonlinear behavior (geometry and material) and buckling are considered in TO. The objective function is the sum of reaction forces. A monotonic loading equal to 120 mm displacement in the right direction is applied to the models.

It was shown that small holes do not have very little effect on the SPSWs behavior with moment frame (Alavi and Nateghi 2013). In this paper, the total area of the openings is equal to 50% of the total area of the original plate. So, the volume fraction of plate in the optimization process is considered 0.5. Also, the symmetry of plate about both axes (horizontal and vertical) at the center of the plate is considered.

The sensitivity-based method is used for TO. Sensitivity method is a general algorithm that could be used for structural and non-structural problems with large scale. Also, various types of objective function could be applied to this method (Bendsøe and Sigmund 2003, TOSCA 2013). In the sensitivity analysis, the density (design variables) of all elements is reduced to the predicted volume fraction. In the next step, the FE analysis is done and based on the objective function, the effective elements are recognized using sensitivity analysis. The effective elements must be retained and the other elements must be eliminated. For this purpose, the SIMP (Simple Isotropic Material with Penalization) method is utilized for implementation of material interpolation. This method is a power law to interpolate the density of material based on the penalization (p). The studies showed that the best value for penalization is equal to 3 (Bendsøe and Sigmund 2003). In each iteration, the method of moving asymptotes (MMA) (Svanberg 1987) is used as the mathematical programming to update the design variables. In this method, a strictly convex approximation sub-problem is generated and solved in each step of the iteration. In general, according to the maximization of the sum of reaction forces as the objective function (Θ) and SIMP method, the TO formulation could be written as follows (Eq. (2))

$$\max:\Theta=\sum K_j U$$
$$subjected\ to:\begin{cases} U=K^{-1}F \ \ where\ K=\sum \rho_e^p k_e \\ \dfrac{V(x)}{V_0}\le f \ \ where\ V(x)=\sum \rho_e v_e \\ 0\le \rho_{\min}\le \rho_e \le 1 \end{cases} \tag{2}$$

where j is the node or nodes that constrained by the fixed support (the nodes in the fixed support zone). K_j corresponds to a row of the global stiffness matrix (K) that belonging to the node j considering to the loading direction, U is the global displacements vector, F is the global external forces vector, k_e, v_e and ρ_e are the element stiffness, volume and density respectively, $V(x)$ and V_0 are the material volume and design domain volume, respectively, f is the prescribed volume fraction (f = 0.5), and p is the penalization power according to the SIMP method (p = 3).

In fact, no element in TO is eliminated, but its density decreases. If any of the elements are removed, in each iteration, the mesh must be renewed, which is very time-consuming. On the other hand, the density of the element cannot be equal to zero because it causes a singularity in the problem-solving. So, a minimum density ($\rho_{\min}$) for each element must be defined. Herein, the minimum density is equal to 0.001.

MMA approximates a function (ψ) of m real variables $x = (x_1, \dots, x_m)$ around a given iteration point x^0 by Eq. (3)

$$\psi(x)\approx\psi(x^0)+\sum_{i=1}^{m}\left(\frac{r_i}{U_i-x_i}+\frac{s_i}{x_i-L_i}\right)$$
$$\text{subjected to:}$$
$$\begin{cases} \text{if } \dfrac{\partial\psi}{\partial x_i}>0\Rightarrow r_i=(U_i-x_i^0)^2\dfrac{\partial\psi}{\partial x_i}(x^0) \text{ and } s_i=0 \\ \text{if } \dfrac{\partial\psi}{\partial x_i}<0\Rightarrow r_i=0 \text{ and } s_i=-(x_i^0-L_i)^2\dfrac{\partial\psi}{\partial x_i}(x^0) \end{cases} \tag{3}$$

where U_i and L_i are the upper and lower of vertical asymptotes for the approximations of ψ.

The optimization is performed iteratively until one of the stop conditions is satisfied. The number of total iterations is the first stop condition. The changes of the configuration in the TO iterations are very small and ignorable when the rate changes of the objective function and elements density are very decreased. So, to prevent the doing of extra iterations, the rate changes of the objective function (l_1) and average changes of elements density (l_2) are considered as the stop conditions as follow

$$\frac{\left|\Theta_{n+1}-\Theta_n\right|}{\left|\Theta_{n+1}\right|}\le l_1 \tag{4}$$

$$\frac{\left|\rho_{n+1}-\rho_n\right|}{N}\le l_2 \tag{5}$$

where n is the number of iterations and N is the total number of elements.

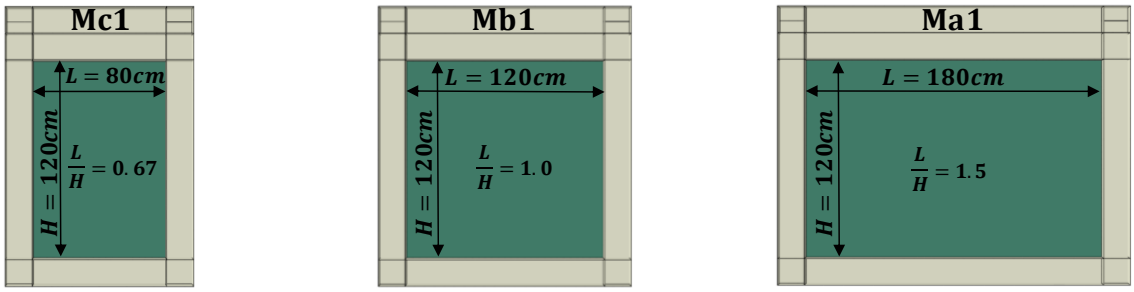

(a) Aspect ratio = 0.67 (b) Aspect ratio = 1.0 (c) Aspect ratio = 1.5

Fig. 7 Initial model for topology optimization

In this paper the maximum number of iterations is equal to 100, the maximum rate change of the objective function is equal to l_1 = 0.001 and the maximum average change of elements density is equal to l_2 = 0.003. Also, at least four iterations must be conducted to terminate the TO. It should be noted that the number of iterations and the values of stop conditions are determined using trial and error on the models to obtain a clear optimized topology.

4. Topology optimization scenarios and results

Three Length-to-Height (L/H) ratios of the plate are defined for TO that are based on the presented model in the second section. Two popular amounts of length-to-height ratio in the buildings are equal to 1.0, 1.5. Also, around the stair boxes is one of the suitable positions for placing the bracing or SPSW but, the length-to-height ratio is usually less than 1.0. As shown in Fig. 7, the amounts of aspect ratios (L/H) are respectively equal to 0.67 (Mc1), 1.0 (Mb1) and 1.5 (Ma1). Also, three thicknesses for each aspect ratio are considered. According to FEMA450 (2003), the minimum and maximum plate thickness are equal to Eq.6 and Eq. (7) respectively.

$$25\sqrt{\frac{E}{f_y}} > \frac{\min(H,L)}{t_w} \Rightarrow t_{w(\min)} > \frac{\min(H,L)}{25}\sqrt{\frac{f_y}{E}} \quad (6)$$

$$t_{w(\max)} < \frac{LI_c}{0.00307H^4} \quad (7)$$

where t_w is the plate thickness, H is the height of plate, L is the length of plate, f_y is the specified minimum yield stress, E is elastic modulus and I_c is the moment of inertia of the column. Minimum thickness is equal to 1.13 for 0.67 and 1.69 for 1.0 and 1.5 aspect ratios. The maximum plate thicknesses for 0.67, 1.0 and 1.5 aspect ratio are respectively equal to 3.2 mm, 4.7 mm and 7.04 mm. Therefore, the defined thicknesses for the perforated plates

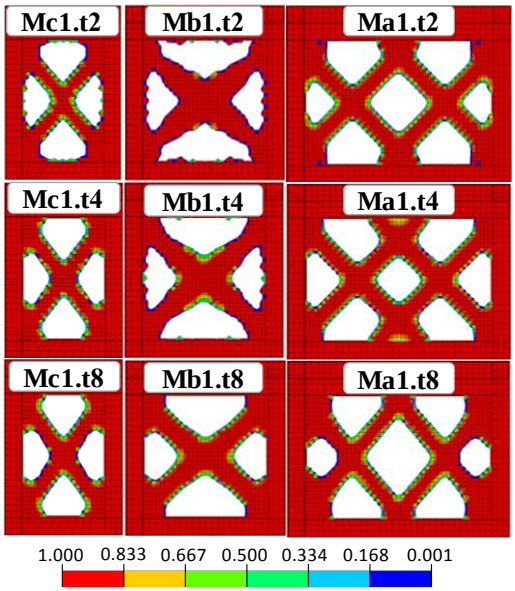

Fig. 8 The results of TO for plate with 8 mm thickness

Table 2 Topology optimization definitions and results

Model name	Aspect ratio	Plate thickness (mm)	Initial volume fraction	Final volume fraction	Initial objective function (kN)	Final objective function (kN)	Number of iterations
Mc1.t2	0.67	2	0.5	0.4999	435.43	466.62	78
Mc1.t4	0.67	4	0.5	0.5000	467.86	543.14	80
Mc1.t8	0.67	8	0.5	0.5000	537.85	704.70	77
Mb1.t2	1	2	0.5	0.5000	575.17	617.22	80
Mb1.t4	1	4	0.5	0.4996	613.79	726.21	51
Mb1.t8	1	8	0.5	0.4998	706.65	1018.52	58
Ma1.t2	1.5	2	0.5	0.4999	596.65	685.14	52
Ma1.t4	1.5	4	0.5	0.4999	655.90	835.43	58
Ma1.t8	1.5	8	0.5	0.4997	777.42	1193.50	65

are equal to 2 mm, 4 mm and 8 mm that are named thin, moderate and thick plates respectively. Finally, there are nine scenarios for TO in total. The definitions and results of TO are presented in Table 2.

The results illustrate that TO terminates without carrying the total number of iterations. The maximum number of iterations is equal to 80 that belonged to the Mc1.t4 and Mb1.t2 models. The final optimized configurations are indicated in Fig. 8. The results show that the plate thickness is not considerably impacted on the TO results. It only has a little effect on the model with 1.5 aspect ratio, whose effects are negligible. The results of TO converge to an X-shape as the optimized form of models with aspect ratios 1.0 (Mb1 model) and 0.67 (Mc1 model). The optimized form for aspect ratio 1.5 (Ma1 model) is different and is approximately combined from two X-shapes (XX).

Fig. 8 shows that the density of most of the remaining elements is reached to $\rho_e = 1$ and only a small number of elements have the density of less than $\rho_e < 1$ which are on the edges (the configuration of optimized topology is clear). It proves the determined values for the stop conditions (l_1 and l_2) are suitable and also prevent from the extra iterations considering the time-consuming of the nonlinear analysis in each iteration. As shown in Fig. 8, no slim and inapplicable parts are created by TO in the optimized plates due to nonlinear analysis. The plastic strain and buckling occur in a slim part during a nonlinear analysis. So, it cannot be effective in the maximization of reaction forces and consequently, it is eliminated during iterations by TO.

The TO keeps the effective diagonal folds based on the angle of inclination for maximization of reaction forces (see Fig. 9). Also, the results show that for small amounts of aspect ratio (L/H), a diagonal stripe is sufficient (X-shaped). But, with the increase of aspect ratio and based on the angle of inclination, the TO creates two stripes (XX-shaped) to maximize the reaction forces. Herein, a parametric investigation is done to find an aspect ratio that causes the "X" form to change to the "XX" form. For this purpose, the TO is done for changes in the length with 100 mm increments. The results indicate that in the 1500mm length (L/H = 1.25), the change from "X" to "XX" form occurs (see Fig. 10).

For investigating the optimization process, the changes in the amounts of the objective function and volume fraction for models with the 8 mm plate thickness are presented in Fig. 11. Also, the changes in the plate configuration are shown in Fig. 12. The results indicate the amounts of the objective function in each iteration are increased while the sum of volume fraction during TO is approximately constant (see Fig. 11). Also, the rate of changes in the objective function with the increase of iterations is decreased. As shown in Fig. 12, the amounts of the volume fraction of all elements in the first iteration (zero iteration) are equal to 0.5. With the increase in the iterations, the volume fraction of effective elements in the maximization of the objective function is increased. On the other hand, the volume fraction of ineffective elements is reduced. When the volume fraction of an element is equal to $\rho_{\min}$ (0.001), the element is graphically eliminated. The process of other models in TO is also the same as models with the 8 mm plate thickness so, the presentation of their graphs and figures is ignored.

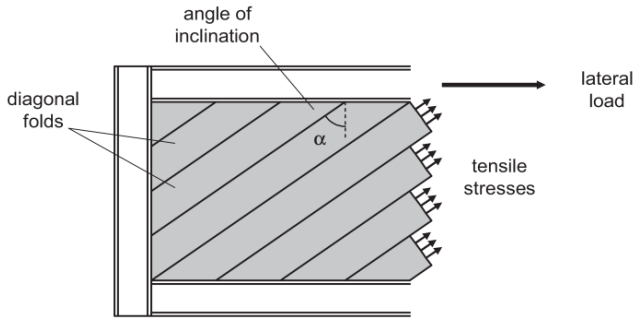

Fig. 9 Idealized tension-field action in a typical SPSW

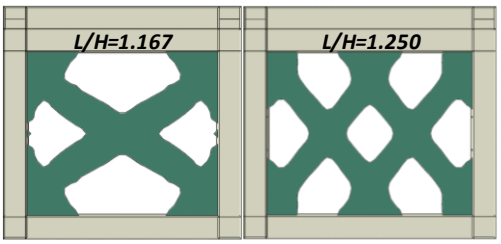

Fig. 10 The changes in the optimized form based on the aspect ratio

5. Nonlinear behavior of optimized plates

In this section, the nonlinear behavior of the optimized plates under cyclic loading is investigated. Also, based on

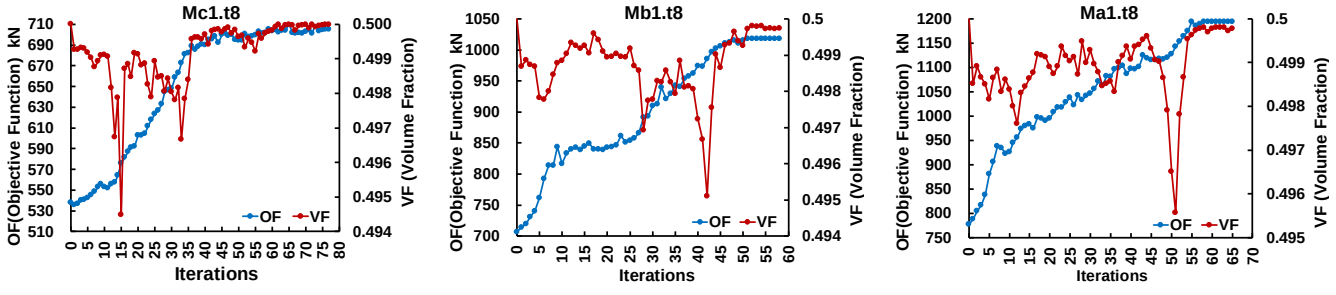

(a) Aspect ratio = 0.67 (b) Aspect ratio = 1.0 (c) Aspect ratio = 1.5

Fig. 11 The values of the objective function and volume fraction during TO for 8mm plate thickness

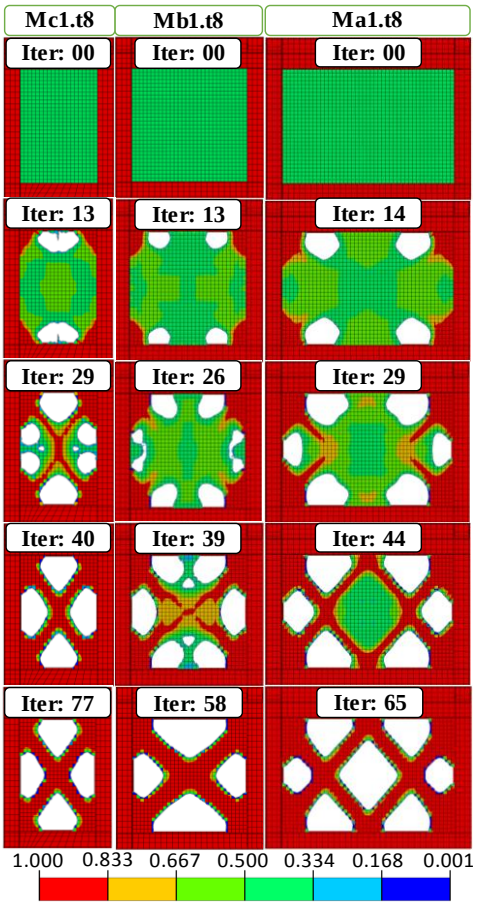

Fig. 12 Configuration of plates with 8 mm thickness during TO

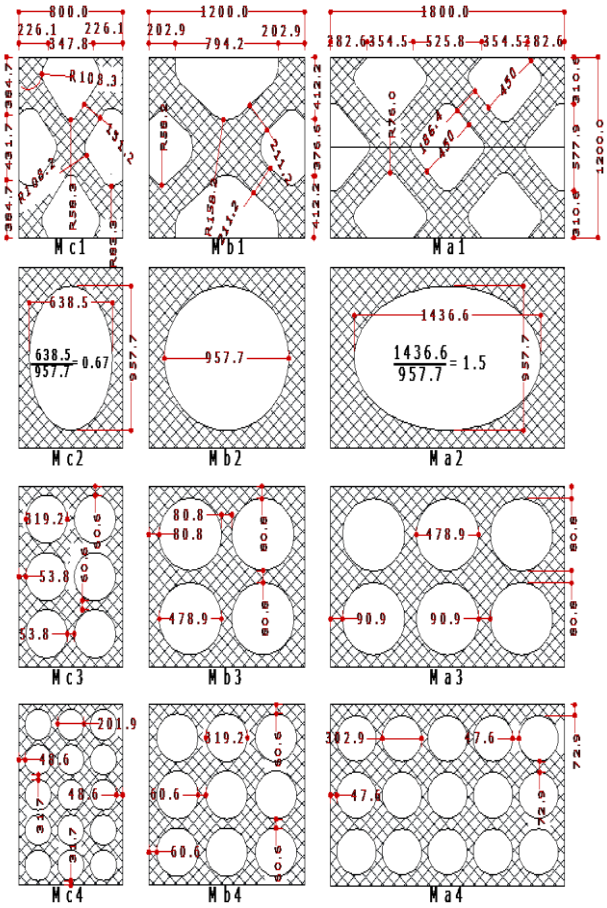

Fig. 13 Optimized and perforated plates dimension (all in millimeter)

Table 3 Introduced models for numerical investigation

	Aspect ratio = 0.67			Aspect ratio = 1			Aspect ratio = 1.5			
	No	Model name	Plate form	No	Model name	Plate form	No	Model name	Plate form	Plate thk (mm)
	1	Mc	No plate	17	Mb	No plate	33	Ma	No plate	-
Thin plate	2	Mc0.t1	Infill plate	18	Mb0.t1	Infill plate	34	Ma0.t1	Infill plate	1
	3	Mc1.t2	Mc1	19	Mb1.t2	Mb1	35	Ma1.t2	Ma1	2
	4	Mc2.t2	Mc2	20	Mb2.t2	Mb2	36	Ma2.t2	Ma2	2
	5	Mc3.t2	Mc3	21	Mb3.t2	Mb3	37	Ma3.t2	Ma3	2
	6	Mc4.t2	Mc4	22	Mb4.t2	Mb4	38	Ma4.t2	Ma4	2
Moderate plate	7	Mc0.t2	Infill plate	23	Mb0.t2	Infill plate	39	Ma0.t2	Infill plate	2
	8	Mc1.t4	Mc1	24	Mb1.t4	Mb1	40	Ma1.t4	Ma1	4
	9	Mc2.t4	Mc2	25	Mb2.t4	Mb2	41	Ma2.t4	Ma2	4
	10	Mc3.t4	Mc3	26	Mb3.t4	Mb3	42	Ma3.t4	Ma3	4
	11	Mc4.t4	Mc4	27	Mb4.t4	Mb4	43	Ma4.t4	Ma4	4
Thick plate	12	Mc0.t4	Infill plate	28	Mb0.t4	Infill plate	44	Ma0.t4	Infill plate	4
	13	Mc1.t8	Mc1	29	Mb1.t8	Mb1	45	Ma1.t8	Ma1	8
	14	Mc2.t8	Mc2	30	Mb2.t8	Mb2	46	Ma2.t8	Ma2	8
	15	Mc3.t8	Mc3	31	Mb3.t8	Mb3	47	Ma3.t8	Ma3	8
	16	Mc4.t8	Mc4	32	Mb4.t8	Mb4	48	Ma4.t8	Ma4	8

the conducted studies, three traditional configurations of PSPSW, a model with infill plate and a frame without plate are presented and their results are compared with the optimized models. Herein, the material volume of optimized, perforated and infill plates for similar aspect ratio and thickness is equal. As shown in Fig. 13, three traditional perforated plates are presented including a plate with a central hole and two plates with multi holes for each aspect ratio. According to the equality in the material volume of the plates, the effects of enhancement of the holes number and the reduction of holes diameter in the cyclic behavior are investigated and compared with the optimized plates. Considering the increase in manufacturing costs of the optimized and perforated plates with multi holes, the use of them should be led to improvements in the cyclic behavior. Also, considering the plates thickness and changes in the strength and ductility, the use of the perforated plates replacing the infill plate should be reasonable. In addition, the effects of plate thickness and aspect ratio are significant in the cyclic nonlinear behavior. Therefore, a comprehensive comparison is required for judging and deciding to select a type of shear plate model with respect to the aspect ratio and plate thickness.

The dimensions of the optimized and perforated plates are indicated in Fig. 13. For nonlinear analysis of each model under cyclic loading, a finite element model is produced using ABAQUS. Excluding the mesh size and fish plate (PL 70x5), all parameters and details of modeling (loading pattern, element type, analysis, etc.) are according to the prescribed details in the second section. The mesh size of perforated plates is reduced to 15 mm. In addition, the mesh size of frame is equal to 40 mm. In the modeling, the fish plate (PL 70x5) is ignored. The area of perforated plates for each aspect ratio is similar and equal to 50% of the infill plate. For each amount of aspect ratio, three plates with 2 mm, 4 mm, and 8 mm thicknesses are defined. So, the total number of models is equal to 48. The thickness of the infill plates is reduced by half in order to equalize the material volume of perforated and infill plates with identical aspect ratio. The name of models, plate forms and thicknesses are presented in Table 3.

5.1 Strength capacity

The cyclic behavior of the models is presented in Fig. 14. As expected, the strength is enhanced by the increase of aspect ratio and plate thickness. Also, the difference in strength between the infill plate (black line) and optimized plate (red line) is enhanced by the increase of aspect ratio and plate thickness. It can be seen from Fig. 14 that the infill and optimized plate have the highest reaction forces respectively. To better view curves, the force-deformation curves of the last loop for 1.5 aspect ratio are presented in Fig. 15. As shown in Fig. 15, the main difference between the strength of the optimized and perforated plates is observed in the tension field zone. There is no significant difference between the optimized and perforated plates in the pinching zone. It can be seen that in the pinching zone, the strength of the optimized and perforated plates with 2 mm and 4 mm thicknesses is equal to frame without the plate. It means that in the pinching zone, the strength of plates is not effective and the main contribution of the

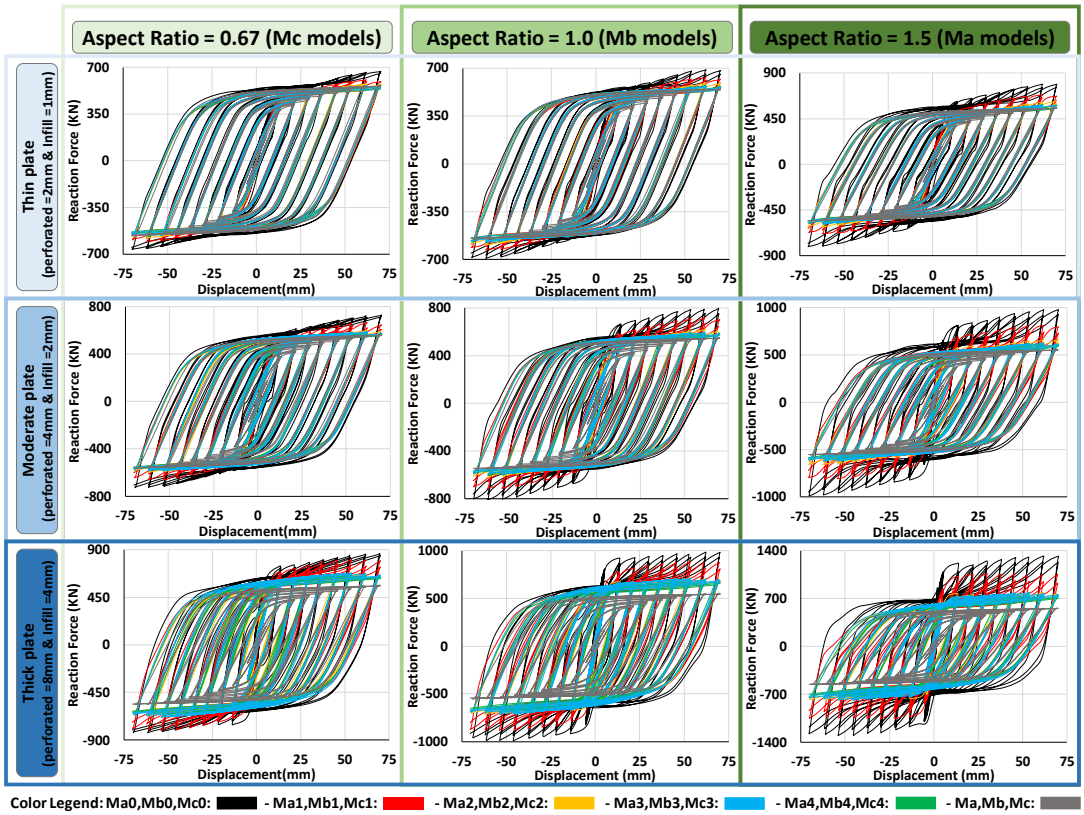

Fig. 14 Force-deformation curve of models under cyclic loading

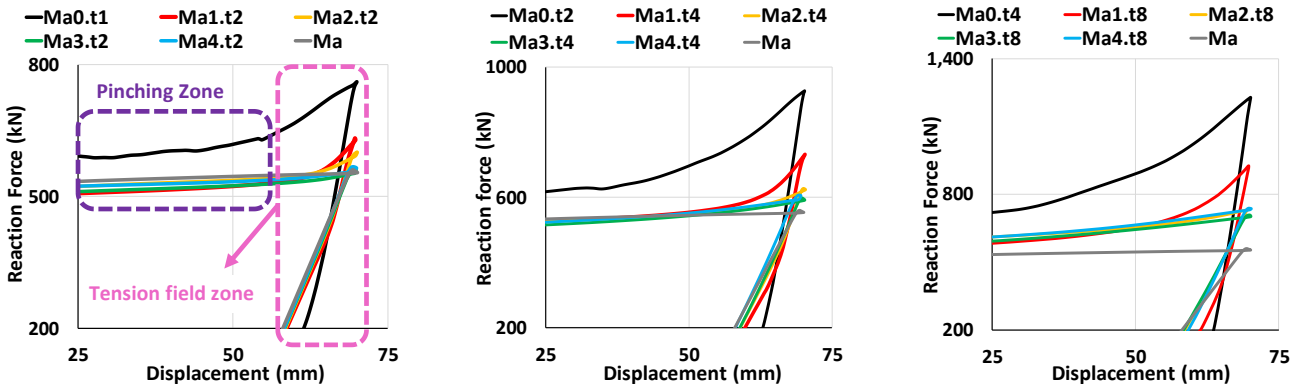

(a) Thin plate (b) Moderate plate (c) Thick plate

Fig. 15 Force-deformation curves in the last loop for 1.5 aspect ratio

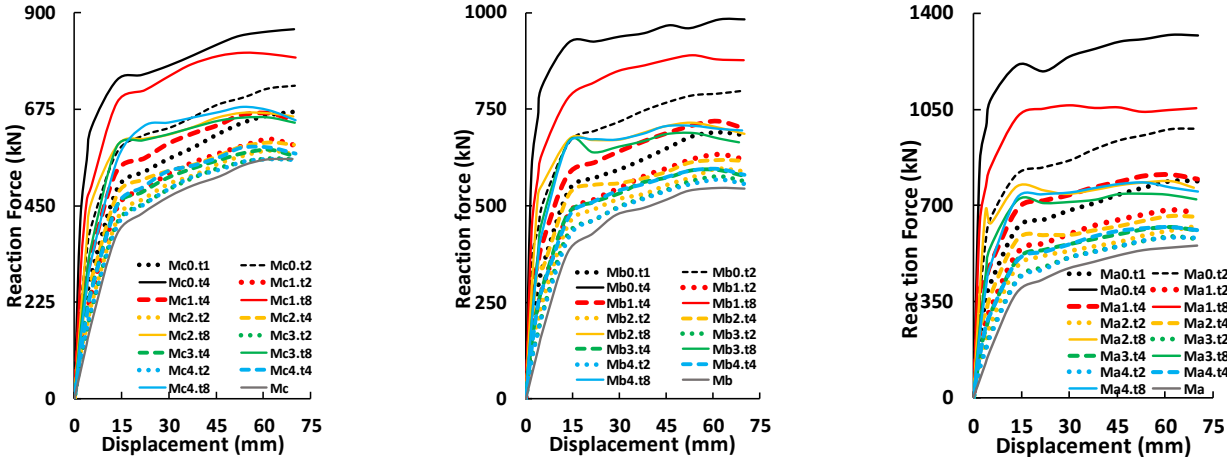

(a) Aspect ratio = 0.67 (b) Aspect ratio = 1.0 (c) Aspect ratio = 1.5

Fig. 16 Push of force-deformation curves

strength of frame is provided with the moment connections. But, with the increase of plate thickness to 8mm, the optimized and perforated plates increase the strength of frame in the pinching zone.

The push of cyclic curves is presented in Fig. 16. In comparison with the other perforated plates, the results illustrate the optimized plates improve the strength and stiffness effectively for all aspect ratios and plate thicknesses. It can be seen from Fig. 16 that the Ma1.t4 with 4mm thickness has more strength than the Ma2t8, Ma3t8 and Ma4.t8 models with 8mm thickness (at the end of cyclic loading). This situation is also occurred for Ma1.t2 and the other aspect ratios. The strength differences between infill plate and optimized plate (Ma1, Mb1 and Mc1) are considerable. This strength difference is minimum in the models with 0.67 aspect ratio, especially with 8 mm thickness.

5.2 Energy dissipation

The energy dissipation of a structure under the cyclic loading is equal to the area bounded by the cyclic curve. The energy dissipation of the models is shown in Fig. 17. In the energy capacity similar to strength capacity, the values of the energy in the models with infill plate are more than the perforated plate. Also, the optimized models have the highest values of energy in comparison to the other perforated models.

5.3 Fracture tendency

Herein, it is necessary to investigate the situation of models in the aspect of the plastic strain and fracture tendency. The equivalent plastic strain (PEEQ) is used to predict the local ductility and fracture tendency of steel (ABAQUS 2014, Wang *et al*. 2015) according to Eq. (8).

$$PEEQ = \tilde{\bar{\varepsilon}}^{pl}\Big|_0 + \int_0^t \dot{\tilde{\bar{\varepsilon}}}^{pl} dt \,.\, \dot{\tilde{\bar{\varepsilon}}}^{pl} = \sqrt{\frac{2}{3}\dot{\varepsilon}^{pl}.\dot{\varepsilon}^{pl}} \tag{8}$$

where $\dot{\varepsilon}^{pl}$ is the rate of plastic flow, $\dot{\tilde{\bar{\varepsilon}}}^{pl}$ is the equivalent plastic strain rate, $\dot{\tilde{\bar{\varepsilon}}}^{pl}|_0$ is the initial equivalent plastic strain rate and t is the time duration of the analysis.

The values of PEEQ are presented in Table 4. Also, the values of the maximum reaction force during the cyclic loading (Pn) and the energy (En) at the end of loading are indicated in Table 4. The results indicate the maximum

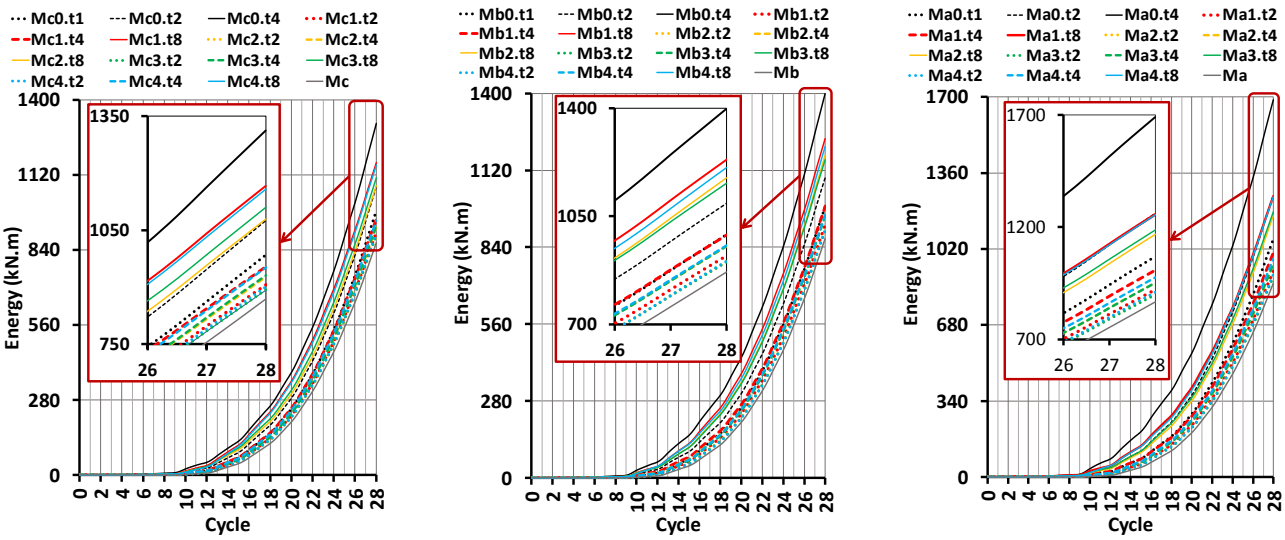

(a) Aspect ratio = 0.67 (b) Aspect ratio = 1.0 (c) Aspect ratio = 1.5

Fig. 17 Energy dissipation of models

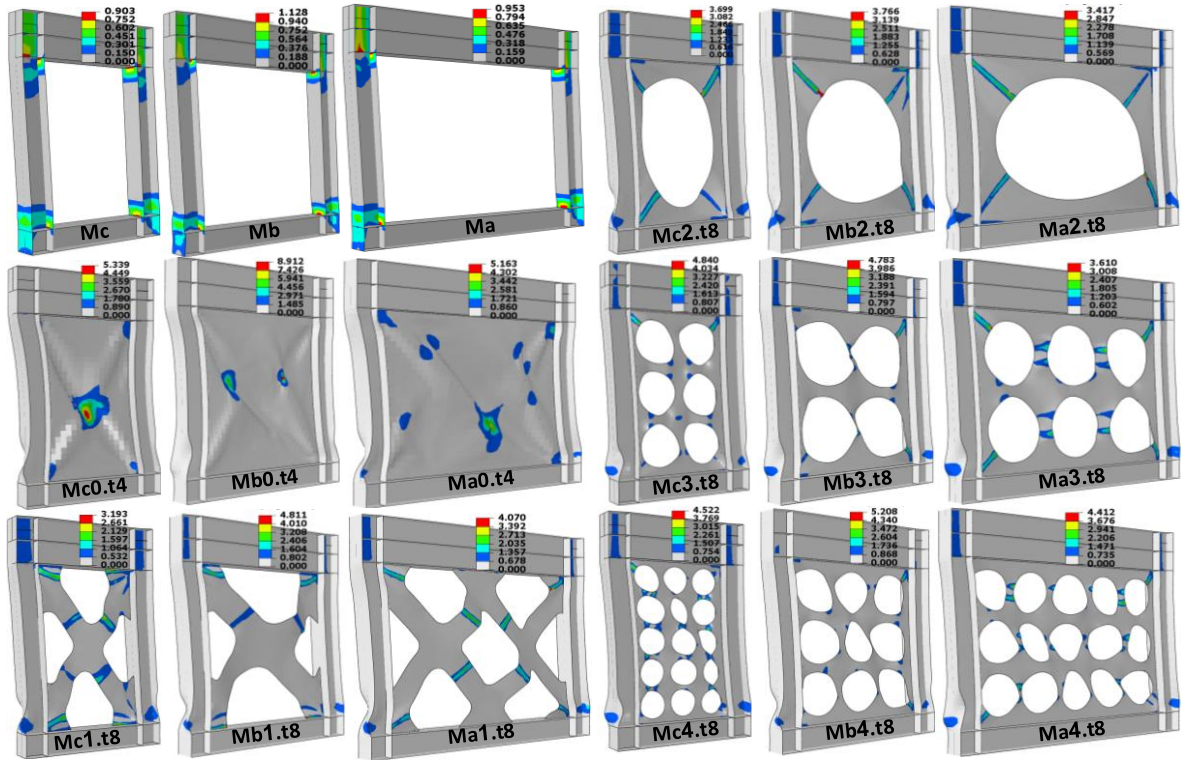

Fig. 18 Deformed shape and PEEQ contour of models at the end of loading

amount of PEEQ belongs to Mb0.t4 (8.912). In the optimized corresponding model (Mb1.t8), the values of Pn and En are reduced by near 10% and 11% respectively. This is while the amount of PEEQ (4.811) is reduced near 46%. After Mb0.t4, Mc0.t4 has the maximum amount of PEEQ (5.339). As shown in Table 4, the amounts of Pn and En for Mc1.t8 are reduced near 6% and 11% respectively comparing with Mc0.t4, while the amount of PEEQ is reduced near 40%. Ma0.t4 has the maximum value of Pn (1321 kN) and En (1689 kN.m). There is a reduction near 19% for Pn and 25% for En in the optimized corresponding model (Ma1.t8). The amount of PEEQ is decreased near 21% comparing to Ma0.t4.

The PEEQ reduction could be observed in the optimized plates with the 4 mm thickness in comparison to infill plate with 2 mm thickness. This reduction is near 28% for Mb1.t4 in comparison to Mb0.t2 while Pn and En are just decreased near 11% and 9% respectively. For Mc1.t4 and Ma1.t4, the amounts of PEEQ are respectively reduced near 2% and 9% in comparison to Mc0.t2 and Ma0.t2 respectively. In the models with the thin plate, there is no fracture tendency improvement observed in the optimized and perforated

Table 3 Introduced models for numerical investigation

	Aspect ratio = 0.67				Aspect ratio = 1				Aspect ratio = 1.5			
	Model name	Pn (kN)	En (kN.m)	PEEQ	Model name	Pn (kN)	En (kN.m)	PEEQ	Model name	Pn (kN)	En (kN.m)	PEEQ
	Mc	565	868	0.903	Mb	555	870	1.128	Ma	561	866	0.953
Thin plate	Mc0.t1	670	984	1.318	Mb0.t1	661	991	1.388	Ma0.t1	750	1068	1.39
	Mc1.t2	606	906	1.783	Mb1.t2	633	922	2.934	Ma1.t2	684	921	1.816
	Mc2.t2	582	891	1.833	Mb2.t2	597	904	3.038	Ma2.t2	626	905	1.981
	Mc3.t2	569	892	1.662	Mb3.t2	578	902	2.003	Ma3.t2	596	899	1.796
	Mc4.t2	566	901	1.86	Mb4.t2	576	906	1.959	Ma4.t2	587	910	1.679
Moderate plate	Mc0.t2	731	1076	2.36	Mb0.t2	808	1092	3.701	Ma0.t2	990	1261	2.546
	Mc1.t4	665	953	2.306	Mb1.t4	719	990	2.652	Ma1.t4	817	1007	2.31
	Mc2.t4	602	927	2.065	Mb2.t4	623	952	2.428	Ma2.t4	663	951	2.155
	Mc3.t4	585	931	1.929	Mb3.t4	606	953	2.549	Ma3.t4	625	953	2.393
	Mc4.t4	591	951	3.112	Mb4.t4	596	956	2.545	Ma4.t4	627	976	3.731
Thick plate	Mc0.t4	863	1312	5.339	Mb0.t4	990	1400	8.912	Ma0.t4	1321	1689	5.163
	Mc1.t8	808	1166	3.193	Mb1.t8	889	1234	4.811	Ma1.t8	1064	1256	4.07
	Mc2.t8	674	1080	3.699	Mb2.t8	716	1174	3.766	Ma2.t8	790	1169	3.417
	Mc3.t8	669	1110	4.84	Mb3.t8	693	1158	4.783	Ma3.t8	747	1187	3.61
	Mc4.t8	685	1158	4.522	Mb4.t8	714	1207	5.208	Ma4.t8	787	1254	4.412

plates in comparison to the infill plates. It means that the use of perforated plate with the thin plate is not preferred unless the opening in the steel wall is needed.

The deformed shape and failure modes at the end of cyclic loading for the models with the thick plate are presented in Fig. 18. It can be seen that in the models without plate, the plastic strain is formed in the column-beam connection and by adding the plate, the plastic strain is moved to the shear plate. In the perforated plates, the plastic strain is distributed in the corners of the plates and the strips around the holes. But, in the infill plates, the plastic strain is approximately concentrated in the center of plates. For this reason, the values of PEEQ are increased in the infill plate. Herein, the presentation of deformed shape for the models with the moderate and thin plates is ignored considering the similarity of their deformed shape with the

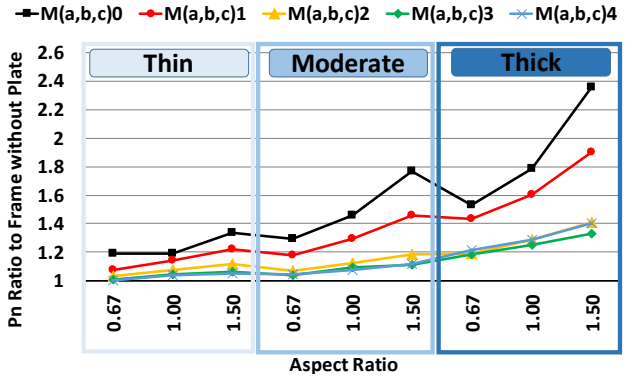

Fig. 19 Comparing the maximum reaction force of models based on the moment frame without plate

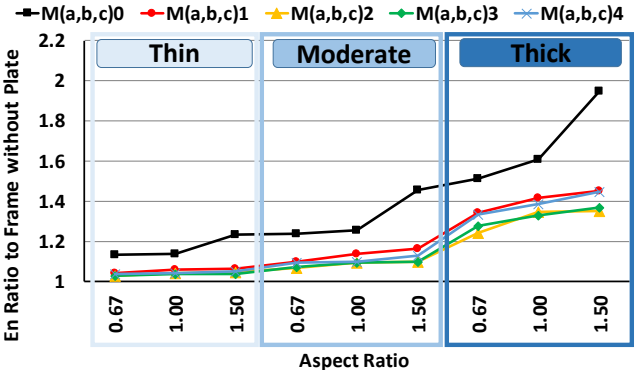

Fig. 20 Comparing the energy dissipation of models based on the moment frame without plate

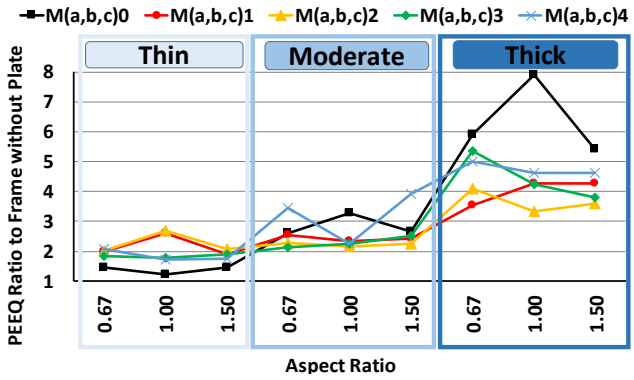

Fig. 21 Comparing the PEEQ of models based on the moment frame without plate

thick plates.

5.4 Summary of nonlinear analysis results

The amounts of the strength, energy and PEEQ of the models are respectively presented in Figs. 19, 20 and 21 relative to the frames without the plate. As shown in Fig. 19, the optimized models for all thicknesses after the models with the infill plate have the maximum strength. Also, the difference of maximum reaction forces between the traditional perforated plates is limited. It means that the effects of the traditional holes in the strength capacity are negligible. However, the plates with the central circle or ellipse have the maximum strength in comparison to the traditional perforated plates.

It can be seen from Fig. 20 that the amounts of energy in the optimized plates are more than perforated plates. In the models with thin plates, the difference of energy between optimized and perforated plates is little. With the increase in the plate thickness, the difference of amounts of energy in the optimized plates in comparison to the traditional perforated plates gradually begins to increase. There is a considerable difference between the amounts of energy for infill plates and perforated plates.

Fig. 21 shows that in the models with the thin plate, the infill plates have the lowest amounts of PEEQ. On the other hand, the infill plates with moderate and thick thickness have the highest amounts of PEEQ. There is no regular and exact process about of PEEQ values of the optimized and perforated plates. However, in general, it can be said that the optimized plates have an appropriate behavior in comparison of the perforated plates.

It is observed that between the traditional perforated plates, the plates with a central circle or ellipse have appropriate behavior in the strength, energy capacity and fracture tendency in comparison with the other traditional perforated plates. In addition, these types of perforated plates are less costly and more simple in terms of cutting and manufacturing.

6. Conclusions

In this paper topology optimization is applied to find a new form of PSPSWs. The study is done in two phase. In the first phase, the topology of plates is optimized based on the reaction force. In the second phase, the nonlinear behavior of optimized plates under cyclic loading is investigated and compared with the four types of SPSWs. Achievements in the optimization phase are as follows:

- The results illustrated that for 0.67 and 1.0 aspect ratios, the plate thickness wasn't impacted on the TO results. The effects of plate thickness weren't significant for 1.5 aspect ratio and were ignored.
- TO for 0.67 and 1.0 aspect ratios, created an X-shape for the plates. For 1.5 of aspect ratio, a combined form of a double X-shaped (XX) was obtained. The area of optimized plates was equal to 50% of the infill plate.
- The study showed that for aspect ratio more than 1.25 ($H/L \geq 1.25$), the X-shape changed to XX-shaped form.

In order to investigate the nonlinear behavior of optimized plates, a frame without plate, an infill plate, a plate with a circle in the center and two multi circle plates were defined. So, 48 models were created and analyzed in total. The volume of all plates with similar thickness and aspect ratio was equal. Achievements in the second phase are as follows:

- The results showed that the optimized models have the highest amounts of strength and energy between the perforated plates. The difference between strength and energy of the infill plates and perforated plates was considerable.
- In the perforated plates with the thick (8 mm) and moderate (4 mm) plates, the fracture tendency (PEEQ) was reduced effectively in comparison to the infill plates (4 mm and 2 mm). The fracture tendency of the optimized models was suitable. It was reduced near 21%~46% for thick and 2%~28% for moderate plates.
- It is noteworthy that the models with thin (1 mm) and infill plates had the lowest fracture tendency while they had higher amounts of strength and energy. Therefore, the use of thin perforated plates is justified if the openings are needed.

References

ABAQUS (2014), Analysis User's Manual, V.6-14, Dassault Systèmes Simulia, Providence, RI, USA.

AISC360 (2010), Specification for Structural Steel Buildings, American Institute of Steel Constructions, Chicago, IL, USA.

Alavi, E. and Nateghi, F. (2013), "Experimental study on diagonally stiffened steel plate shear walls with central perforation", *J. Constr. Steel Res.*, **89**, 9-20.

ATC24 (1992), Guidelines for cyclic seismic testing of components of steel structures for buildings, Applied Technology Council, Redwood City, CA, USA.

Banh, T.T., Shin, S. and Lee, D. (2018), "Topology optimization for thin plate on elastic foundations by using multi-material", *Steel Compos. Struct., Int. J.*, **27**(2), 177-184.

Bendsøe, M.P. and Kikuchi, N. (1988), "Generating optimal topologies in structural design using a homogenization method", *Comput. Meth. Appl. Mech. Eng.*, **71**(2), 197-224.

Bendsøe, M. and Sigmund, O. (2003), *Topology Optimization: Theory, Methods, and Applications*, Springer-Verlag Berlin Heidelberg, New York, NY, USA.

Bhowmick, A.K., Grondin, G.Y. and Driver, R.G. (2014), "Nonlinear seismic analysis of perforated steel plate shear walls", *J. Constr. Steel Res.*, **94**, 103-113.

Chan, R., Albermani, F. and Kitipornchai, S. (2011), "Stiffness and strength of perforated steel plate shear wall", *Proced. Eng.*, **14**, 675-679.

Das, R., Jones, R. and Xie, Y.M. (2011), "Optimal topology design of industrial structures using an evolutionary algorithm", *Optim. Eng.*, **12**(4), 681-717.

Dehghani, M., Mashayekhi, M. and Salajegheh, E. (2016), "Topology optimization of double-and triple-layer grids using a hybrid methodology", *Eng. Optim.*, **48**(8), 1333-1349.

FEMA450 (2003), NEHRP Recommended Provisions and Commentary for Seismic Regulations for New Buildings and

Other Structures, Federal Emergency Management Agency, Washington, D.C., USA.

Formisano, A., Lombardi, L. and Mazzolani, F.M. (2016), "Perforated metal shear panels as bracing devices of seismic-resistant structures", *J. Constr. Steel Res.*, **126**, 37-49.

Gharehbaghi, S., Moustafa, A. and Salajegheh, E. (2016), "Optimum seismic design of reinforced concrete frame structures", *Comput. Concr., Int. J.*, **17**(6), 761-786.

Gholizadeh, S. and Barati, H. (2014), "Topology optimization of nonlinear single layer domes by a new metaheuristic", *Steel Compos. Struct., Int. J.*, **16**(6), 681-701.

Jansseune, A. and Corte, W.D. (2017), "The influence of convoy loading on the optimized topology of railway bridges", *Struct. Eng. Mech., Int. J.*, **64**(1), 45-58.

Kabus, S. and Pedersen, C.B.W. (2012), "Optimal Bearing Housing Designing Using Topology Optimization", *J. Tribol.*, **134**(2), 1-9.

Khatibinia, M., Roodsarabi, M. and Barati, M. (2018), "Topology optimization of plane structures using binary level set method and isogeometric analysis", *Int. J. Optim. Civil Eng.*, **8**(2), 209-226.

Kutuk, M.A. and Gov, I. (2014), "Optimum bracing design under wind load by using topology optimization", *Wind Struct., Int. J.*, **51**(1), 39-66.

Kutyłowski, R. and Rasiak, B. (2014), "Application of topology optimization to bridge girder design", *Struct. Eng. Mech., Int. J.*, **51**(1), 39-66.

Lee, D., Shin, S., Lee, J. and Lee, K. (2015), "Layout evaluation of building outrigger truss by using material topology optimization", *Steel Compos. Struct., Int. J.*, **19**(2), 263-275.

Lu, X., Xu, J., Zhang, H. and Wei, P. (2017), "Topology optimization of the photovoltaic panel connector in high-rise buildings", *Struct. Eng. Mech., Int. J.*, **62**(4), 465-475.

Mashayekhi, M., Salajegheh, E. and Dehghani, M. (2016), "Topology optimization of double and triple layer grid structures using a modified gravitational harmony search algorithm with efficient member grouping strategy", *Comput. Struct.*, **172**, 40-58.

Matteis, G.D., Sarracco, G. and Brando, G. (2016), "Experimental tests and optimization rules for steel perforated shear panels", *J. Constr. Steel Res.*, **123**, 41-52.

Mustafa, M.A., Osman, S.A., Husam, O.A. and Al-Zand, A.W. (2018), "Numerical study of the cyclic behavior of steel plate shear wall systems (SPSWs) with differently shaped openings", *Steel Compos. Struct., Int. J.*, **26**(3), 361-373.

Nassernia, S. and Showkati, H. (2017), "Experimental study of opening effects on mid-span steel plate shear walls", *J. Constr. Steel Res.*, **137**, 8-18.

Qiao, S., Han, X., Zhou, K. and Ji, J. (2016), "Seismic analysis of steel structure with brace configuration using topology optimization", *Steel Compos. Struct., Int. J.*, **21**(3), 501-515.

Roodsarabi, M., Khatibinia, M. and Sarafrazi, S. (2016a), "Isogeometric topology optimization of structures using level set method incorporating sensitivity analysis", *Int. J. Optim. Civil Eng.*, **6**(3), 405-422.

Roodsarabi, M., Khatibinia, M. and Sarafrazi, S.R. (2016b), "Hybrid of topological derivative-based level set method and isogeometric analysis for structural topology optimization", *Steel Compos. Struct., Int. J.*, **21**(6), 1389-1410.

Shekastehband, B., Azaraxsh, A.A. and Showkati, H. (2017), "Hysteretic behavior of perforated steel plate shear walls with beam-only connected infill plates", *Steel Compos. Struct., Int. J.*, **25**(4), 505-521.

Stromberg, L.L., Beghini, A., Baker, W.F. and Paulino, G.H. (2012), "Topology optimization for braced frames: Combining continuum and beam/column elements", *Eng. Struct.*, **37**, 106-124.

Svanberg, K. (1987), "The method of moving asymptotes - A new method for structural optimization", *Int. J. Numer. Meth. Eng.*, **24**(2), 359-373.

Tang, J., Xie, Y.M. and Felicetti, P. (2014), "Conceptual design of buildings subjected to wind load by using topology optimization", *Wind Struct., Int. J.*, **18**(1), 021-035.

TOSCA (2013), V.8.0, Tosca Structure Documentation, Dassault Systèmes Company, Karlsruhe, Baden-Württemberg, Germany.

Tsavdaridis, K.D., Kingman, J.J. and Toropov, V.V. (2015), "Application of structural topology optimisation to perforated steel beams", *Comput. Struct.*, **158**, 108-123.

Valizadeh, H., Sheidaii, M. and Showkati, H. (2012), "Experimental investigation on cyclic behavior of perforated steel plate shear walls", *J. Constr. Steel Res.*, **70**, 308-316.

Vian, D., Bruneau, M., Tsai, K.C. and Lin, Y.C. (2009), "Special perforated steel plate shear walls with reduced beam section anchor beams. I: Experimental investigation", *J. Struct. Eng.*, **135**(3), 211-220.

Wang, M., Yang, W., Shi, Y. and Xu, J. (2015), "Seismic behaviors of steel plate shear wall structures with construction details and materials", *J. Constr. Steel Res.*, **107**, 194-210.

Zhao, X., Liu, Y., Hua, L. and Mao, H. (2016), "Finite element analysis and topology optimization of a 12000KN fine blanking press frame", *Struct. Multidiscip. Optim.*, **54**(2), 375-389.

Zhiyi, Y., Kemin, Z. and Shengfang, Q. (2018), "Topology optimization of reinforced concrete structure using composite truss-like model", *Struct. Eng. Mech., Int. J.*, **67**(1), 79-85.

Zhou, K. (2016), "Topology optimization of bracing systems using a truss-like material model", *Struct. Eng. Mech., Int. J.*, **58**(2), 231-242.

CC